2026 IEEE International Conference on Robotics and Automation (ICRA 2026)
June 1-5, 2026. Vienna, Austria

Integrated Hydrogel Patterning and Dynamic Microparticle Manipulation Using Optoelectronic Tweezers

Shunxiao Huang[1†], Jingwen Ye[1†], Wenyan Niu[1], Ao Wang[1], Zijin Zeng[1], Chan Li[1], Zaiyang Chen[1], Hongyan Sun[1], Yingjian Guo[1*] and Lin Feng[2*]

***Abstract*— This paper presents an integrated optoelectronic tweezers platform that unifies hydrogel microstructure fabrication with subsequent dynamic microsphere manipulation, enabled by a dual-wavelength optical strategy for seamless and programmable control. Initial tests in low-conductivity aqueous media confirmed high-fidelity OET patterning, with edge roughness below 20 μm. Using a biocompatible GelMA–LAP system, we achieved: (i) precise single-region hydrogel structures (hexagram patterns, average deviation 2.779 μm); (ii) scalable, customizable assemblies of complex topologies, including gear and maze arrays; and (iii) coordinated navigation of single, double, and triple microspheres within hydrogels, with triple-sphere velocity differences $<$0.9 μm/s. This approach overcomes the conventional OET limitation of decoupled photolithography and particle manipulation, integrating structure fabrication with dynamic control. It provides a versatile, reproducible platform for tissue engineering scaffolds, targeted drug delivery, and multi-particle coordination.**

I. INTRODUCTION

Microscale precision patterning and dynamic manipulation of microparticles are crucial in tissue engineering scaffold fabrication, targeted drug delivery, and single-cell analysis [1]–[3]. Optoelectronic tweezers (OET), which operate based on light-induced dielectrophoresis (DEP), offer low-power, non-contact, and programmable manipulation, making them ideal for controlled microscale operations [4]–[7]. Existing studies have predominantly focused on aqueous environments [8]–[10], demonstrating the ability to pattern and transport microparticles; however, their application within biologically relevant hydrogel systems remains largely unexplored [11], [12]. Moreover, conventional microscale experiments typically rely on photolithographically fabricated microchannels followed by liquid injection, resulting in a decoupling between "channel fabrication" and "particle manipulation" and lacking an integrated workflow [13]–[15]. In principle, OET not only enables particle manipulation but can also function as a maskless photolithography tool for generating hydrogel microstructures—a potential that has yet to be fully exploited [16]–[18], limiting its broader application in tissue engineering and drug delivery contexts.

To address these limitations, we developed an OET-based integrated hydrogel microscale manipulation platform, incorporating a dual-wavelength optical strategy and employing a biocompatible gelatin methacryloyl (GelMA)–photoinitiator (LAP) system. This platform enables a fully integrated workflow from high-precision hydrogel formation (single-region, batch, and customizable structures) to dynamic navigation of single or multiple microparticles within the hydrogel. Specifically, 365–405 nm light triggers GelMA photopolymerization for precise hydrogel microstructure fabrication, while $\geq$580 nm light drives dielectrophoretic manipulation of particles, ensuring both structural fidelity and dynamic control.

This approach overcomes the conventional OET bottleneck in which microchannel fabrication and particle manipulation are decoupled, and establishes a biocompatible, programmable integrated platform. Without relying on complex photolithography, it enables tight coupling of hydrogel microstructure formation and microparticle manipulation, providing a feasible technical route for precision tissue engineering scaffolds, targeted drug delivery, and coordinated multi-particle experiments, thereby extending the application potential of OET in biomedical research.

II. SYSTEM AND METHODS

A. Preparation of Hydrogel Solutions

Photopolymerization is the core process for forming GelMA–LAP hydrogels [19], [20]. The photoinitiator lithium phenyl-2,4,6-trimethylbenzoylphosphinate (LAP) generates reactive free radicals under 365–405 nm ultraviolet (UV) irradiation, which in turn initiate the free-radical polymerization of methacryloyl groups on gelatin methacryloyl (GelMA) chains, leading to the formation of a three-dimensional crosslinked network, as illustrated in Fig. 1.

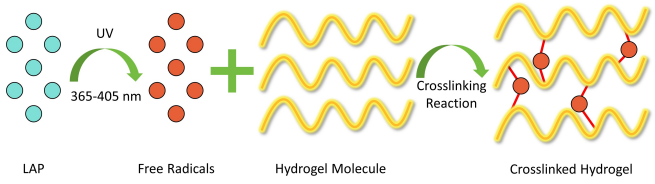

Fig. 1. Schematic illustration of the GelMA crosslinking reaction.

This work was supported by the National Key R&D Program of China (Grant No. 2022YFF1502000), Beijing Municipal Fund for Distinguished Young Scholars (Grand No. JQ22022), and Fundamental Research Funds for the CentralUniversities (YWF-22-K-101).

†These authors contributed equally to this work.

[1]Shunxiao Huang, Jingwen Ye, Wenyan Niu, Ao Wang, Zijin Zeng, Chan Li, Zaiyang Chen, Hongyan Sun, Yingjian Guo are with Beihang University; School of Mechanical Engineering Automation, Beijing, China (e-mail: 13819774497@163.com).

[2]Lin Feng is with Beihang University; Beijing Advanced Innovation Center for Biomedical Engineering and School of Mechanical Engineering Automation, Beijing 100083, China.

*Corresponding author: Lin Feng (e-mail:linfeng@buaa.edu.cn) and Yingjian Guo (e-mail:yingjguo@126.com).

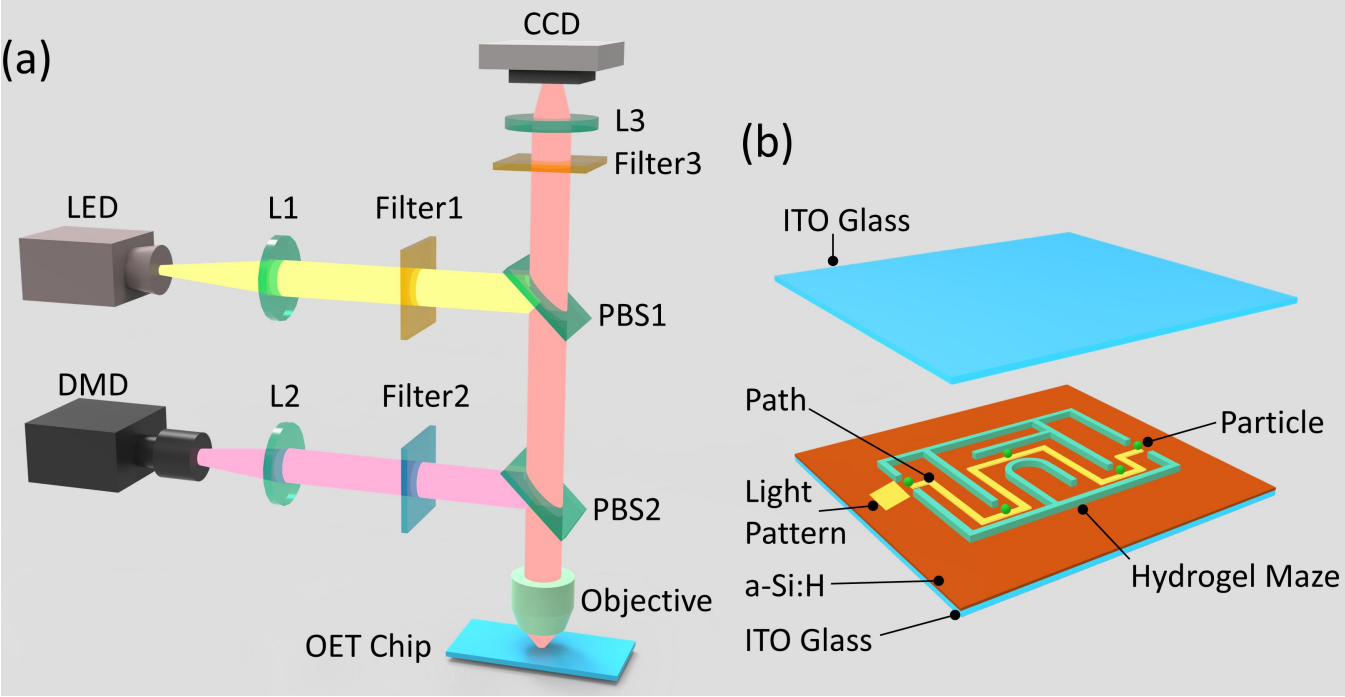

Fig. 2. Schematic overview of the experimental setup: (a) optical path system, (b) OET chip.

To prepare the hydrogel precursor, 0.05 g of LAP powder was dissolved in 20 mL of deionized water to obtain a 0.25% (w/v) LAP stock solution. The solution was incubated in a water bath at 50±1 °C for 15 min with intermittent vortexing to ensure complete dissolution. The stock solution was then sterilized by filtration through a 0.22 μm PES membrane, protected from light, and stored at 4 °C for up to one week to prevent LAP degradation and ensure consistent photopolymerization efficiency.

Subsequently, 1 g of GelMA powder was gradually added to 20 mL of the LAP stock solution. The mixture was heated in a water bath at 70±1 °C for 30 min with intermittent mixing until the GelMA was fully dissolved, forming a homogeneous and transparent solution. This solution was then sterilized again using a 0.22 μm filter. The final hydrogel precursor contained 5% (w/v) GelMA and 0.25% (w/v) LAP. Prior to use, the solution was kept at 37±1 °C to prevent GelMA gelation at low temperatures, which could hinder interactions between functional groups and free radicals. The entire procedure was performed under light protection to avoid premature LAP photolysis and unintended crosslinking.

The conductivity of the prepared hydrogel solution was measured using a Shanghai Leici DDSJ/318T precision conductivity meter. Three parallel measurements yielded an average conductivity of 28.4±0.3 μS/cm.

B. Experimental Setup

The OET system used for microparticle manipulation in this study was a custom-integrated platform, comprising four key modules: optical path system, chip module, electrical driving, and imaging/recording. As shown in Fig. 2(a), the optical path employed a BenQ E580 digital micromirror device (DMD) projector (native resolution 1920×1080, 120 Hz) as a spatial light modulator. Binary light patterns (light region: gray value 255; dark region: gray value 0) were generated via an industrial computer using the OpenCV 4.5.5 platform, and delivered to the DMD through an HDMI 3.0 interface, enabling millisecond-scale light pattern updates. The DMD output passed through a 4f imaging relay system composed of AC254-100-B-ML (focal length 100 mm) and AC254-50-B-ML (focal length 50 mm) lenses for collimation and beam reduction. Switchable optical filters (580 nm high-pass or 450 nm low-pass) were inserted to remove stray light. The final beam was focused onto the chip photoconductive layer using an Olympus UPLFLN10X2PH objective (NA = 0.3), achieving a diffraction-limited spot size of 1.2 μm. System illumination employed a 580 nm LED (Thorlabs M580L3) configured in a Köhler illumination setup to provide uniform background light without contributing to the OET dielectrophoretic effect.

The chip adopted a symmetric sandwich structure, as shown in Fig. 2(b). The top and bottom substrates were 20 mm × 40 mm × 0.7 mm indium tin oxide (ITO) conductive glass (sheet resistance <10 Ω/sq), with the top ITO glass transmittance >90%. The bottom ITO surface was coated with a 2 μm-thick hydrogenated amorphous silicon (a-Si:H) photoconductive layer via plasma-enhanced chemical vapor deposition (PECVD), exhibiting a dark-state conductivity $<10^{-6}$ S/m and a photoconductive gain >100. The chamber was formed using 100 μm-thick PTFE spacer tape (oxygen plasma-treated at 50 W for 30 s to enhance adhesion). Prior to experiments, the chamber was filled with

GelMA–LAP solution containing 15 μm polystyrene (PS) microspheres (density 1.05 g/cm^3) at a concentration of 1×10^4 particles/mL.

Electrical actuation was provided by a RIGOL DG1022Z dual-channel function generator (output impedance 50 Ω), applying a 15 Vpp sinusoidal AC signal (100 kHz–1 MHz) between the bottom a-Si:H layer and top ITO electrode. Imaging and recording were performed using a PointGrey GS3-U3-23S6C-C CCD camera (1920×1080 pixels, 60 fps) with a custom interface. Images were acquired via the FlyCapture SDK and subsequently analyzed for microparticle positions and trajectories using ImageJ in combination with Python scripts.

C. Principle of Optoelectronic Tweezers

The core mechanism enabling precise microparticle manipulation in aqueous and hydrogel environments using OET is light-controlled impedance-modulated DEP [21]. This mechanism can be analyzed from two aspects: physical principles and impedance modulation.

DEP refers to the motion of neutral microparticles in a non-uniform electric field due to polarization, which induces an electric dipole moment and results in an electrostatic force along the field gradient (the DEP force, F_{DEP}). Unlike electrophoresis, which requires net particle charge, DEP depends on the difference in complex permittivity between the particle and the surrounding medium. The degree of particle polarization is characterized by the real part of the Clausius–Mossotti (CM) factor, $\mathrm{Re}[K(\omega)]$, defined as:

$$\mathrm{Re}[K(\omega)] = \mathrm{Re}[\frac{\tilde{\varepsilon}_p - \tilde{\varepsilon}_m}{\tilde{\varepsilon}_p + 2\tilde{\varepsilon}_m}], \tag{1}$$

where $\tilde{\varepsilon} = \varepsilon - j\frac{\sigma}{\omega}$ is the complex permittivity, with ε is the permittivity, σ is the conductivity, $\omega = 2\pi f$ is the angular frequency of the applied field, f is the driving frequency, and j is the imaginary unit. Subscripts p and m represent the PS microsphere and the hydrogel solution, respectively.

When $\mathrm{Re}[K] > 0$, the particle is more polarizable than the medium and moves toward high-field regions (positive DEP, pDEP). Conversely, when $\mathrm{Re}[K] < 0$, the particle moves toward low-field regions (negative DEP, nDEP).

In OET, programmable electric field modulation is achieved via light-induced impedance changes in the a-Si:H photoconductive layer. In the dark state, the a-Si:H layer contains few photo-excited electron–hole pairs, producing a uniform electric field between the top and bottom electrodes. Upon illumination by a light pattern, photons excite electrons, generating free carriers and reducing local impedance. The significant impedance contrast between illuminated and non-illuminated regions creates localized high-field regions at the light–dark boundaries, resulting in a non-uniform electric field.

For a spherical particle of radius r, the dielectrophoretic force is quantitatively expressed as [22]:

$$F_{\mathrm{DEP}} = 2\pi\varepsilon_m r^3 \mathrm{Re}[K(\omega)]\nabla|E|^2, \tag{2}$$

where E is the local electric field intensity. Through this cascade of effects—light pattern leading to impedance modulation, which in turn induces a non-uniform electric field, ultimately resulting in a DEP force—OET enables programmable patterning and manipulation of PS microspheres in both aqueous and hydrogel environments.

III. EXPERIMENTS AND RESULTS

A. Aqueous-Phase Preliminary Experiments: Verification of Programmable OET Patterning

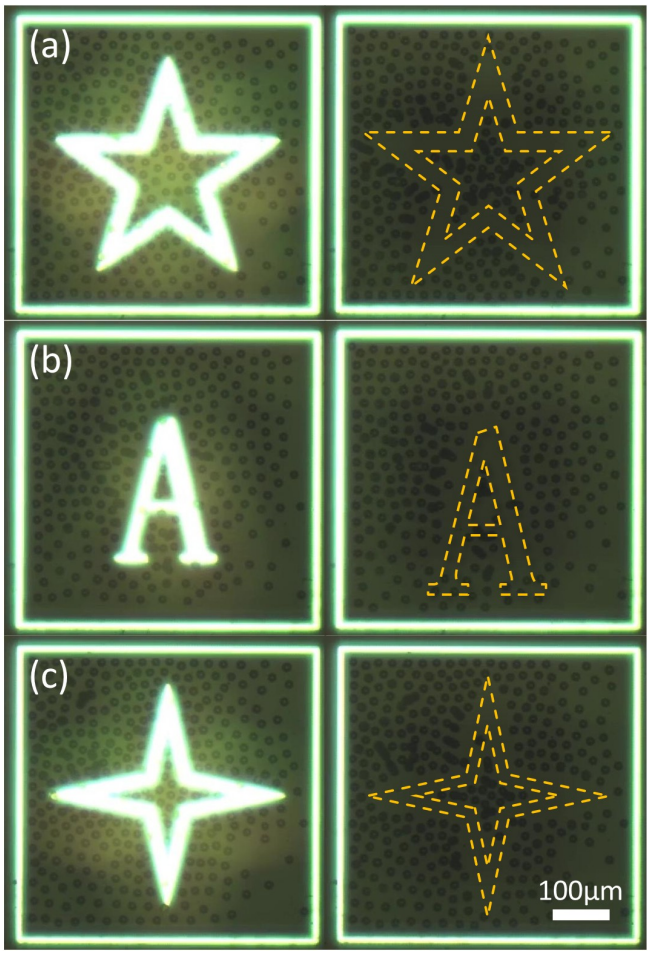

Fig. 3. Programmable patterning of 15 μm PS microspheres in aqueous solution using OET: (a) pentagram, (b) letter “A”, (c) cross star.

To verify the basic feasibility of programmable patterning using OET, preliminary experiments were conducted in an aqueous environment. PS microspheres (15 μm diameter) dispersed in low-conductivity deionized water (0.466 μS/cm) served as the target particles. A 15 Vpp, 100 kHz AC electric field was applied, while customized light patterns were projected in real-time using an DMD to control particle motion.

To ensure uniform microsphere distribution and clear pattern formation, a pre-aggregation strategy was employed to concentrate microspheres in the core region before projecting the target patterns, such as a pentagram, the letter “A”, and a cross star, as shown in Fig. 3. The results demonstrated

that the microspheres formed patterns with sharp edges, exhibiting an edge roughness of <20 μm. The loading and removal of patterns were stable and repeatable over multiple cycles.

These preliminary experiments confirmed that the OET system can achieve high-fidelity and reproducible microparticle patterning in aqueous media, providing a methodological foundation for subsequent static hydrogel microstructure fabrication and dynamic microparticle manipulation.

B. High-Precision Patterning of Single-Region Hydrogel Structures

Following the aqueous-phase preliminary experiments, attention was shifted to a biologically compatible hydrogel environment using the GelMA–LAP system as the matrix. Leveraging the programmable optical control of OET, high-precision hydrogel patterning was achieved. While the process is analogous to maskless photolithography, the combination of GelMA's inherent biocompatibility and the dynamic light-field capability of OET provides an integrated solution meeting the biological requirements of "structure–bioactivity–manipulation compatibility."

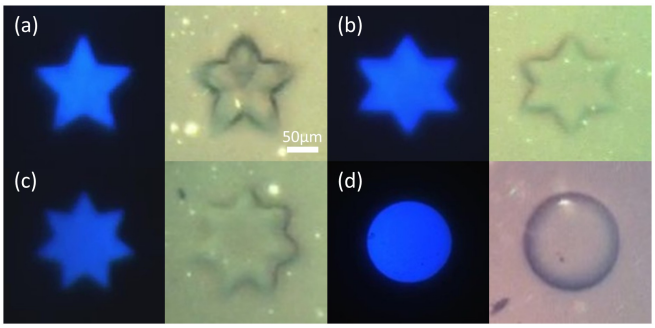

Fig. 4. Single-region hydrogel microstructures generated via OET in GelMA–LAP system: (a) pentagram, (b) hexagram, (c) heptagram, (d) circle.

In the experiments, the prepared GelMA–LAP precursor solution was injected into the OET chip sample chamber. Target light patterns including a pentagram, hexagram, heptagram, and circle (as shown in Fig. 4) were sequentially projected (365–405 nm), triggering LAP photoinitiated GelMA chain crosslinking and polymerization. Illuminated regions solidified to form hydrogel, whereas non-illuminated regions remained liquid, resulting in geometric structures closely matching the projected patterns. Thanks to pixel-level light pattern control and rapid projection, all four target structures were fabricated within approximately 2 minutes.

To quantitatively assess pattern fidelity, the hexagram was selected as an example. Contours of the projected light pattern and the fabricated hydrogel were extracted, and radial angular errors were analyzed, as shown in Fig. 5. Using the geometric center of the hexagram as the origin, rays were cast every 1° from 0° to 360°, and the distance errors between intersections of the projected and fabricated contours were computed. All 360 angles produced valid intersections, indicating 100% contour integrity. The maximum error was 10.458 μm, less than 7% of the hexagram size (150 μm), with a mean error of 2.779 μm and standard deviation of 2.204 μm, demonstrating small and uniform deviations. Other patterns also exhibited high fidelity: pentagram corners were sharp, the heptagram's complex topology was intact, and the circular edge deviation was <10 μm, confirming the precise control capability of OET for hydrogel patterning.

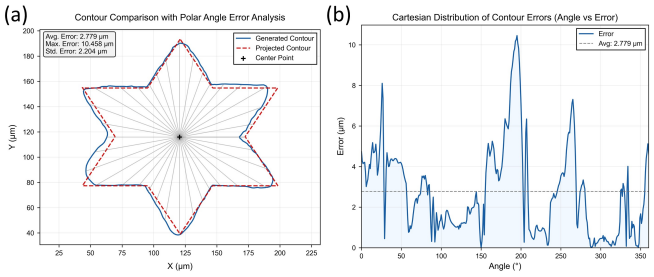

Fig. 5. Quantitative analysis of hexagram hydrogel patterning: (a) comparison between projected light pattern and actual generated hydrogel contour, (b) statistical distribution of contour errors.

Technically, this experiment has several key implications: first, precise selection of 365–405 nm light ensures efficient LAP photopolymerization while minimizing interference with subsequent particle manipulation; second, the biocompatibility and mechanical stability of GelMA hydrogels provide a feasible matrix for constructing cellular microenvironments and tissue engineering scaffolds, forming the structural basis for dynamic microsphere navigation within hydrogel mazes. Compared to the temporary particle arrangements in aqueous-phase experiments, the solidified hydrogel patterns serve as static structural frameworks capable of supporting dynamic particle manipulation, enabling integrated "static pattern–dynamic particle" operations and further extending the application potential of OET in biomedical contexts.

C. Batch and Customized Hydrogel Microstructure Fabrication

Building on the single-region hydrogel patterning experiments, we further evaluated the capability of OET for large-area batch fabrication and customized construction of complex topological microstructures.

To assess batch production performance, a gear-shaped microstructure (single gear: 120 μm $\times$ 120 μm) was employed as the target, as shown in Fig. 6. By projecting an array of light patterns onto the GelMA–LAP precursor solution, multiple microstructures were simultaneously fabricated. Within approximately 10 minutes, more than 50 uniformly sized gears were successfully produced, with inter-gear spacing consistently maintained at 30 μm. These results demonstrate that OET enables multi-region parallel patterning, significantly enhancing microstructure throughput, providing a feasible route for large-scale tissue scaffold fabrication.

To address the demand for "personalized functional carriers" in biomedical applications, we explored the customized generation of complex maze structures to verify the controllability of OET over irregular, large-area patterns. Two maze designs were fabricated:

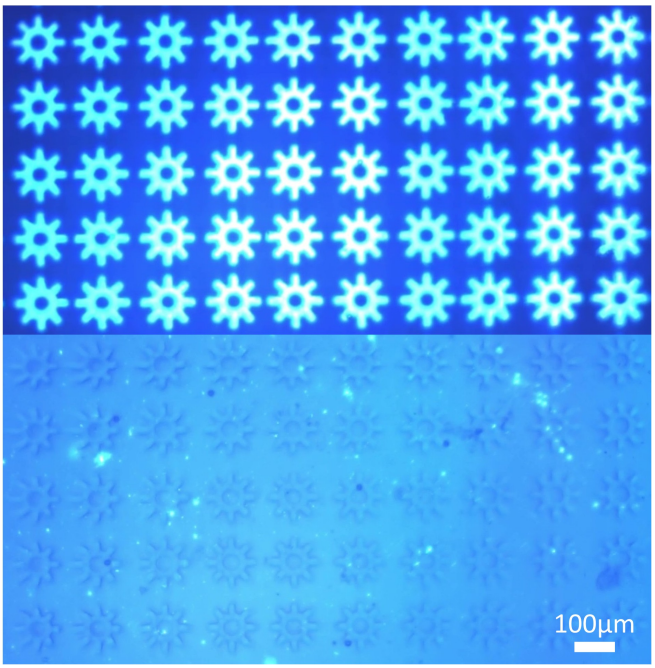

Fig. 6. Batch fabrication of hydrogel gear microstructures using OET.

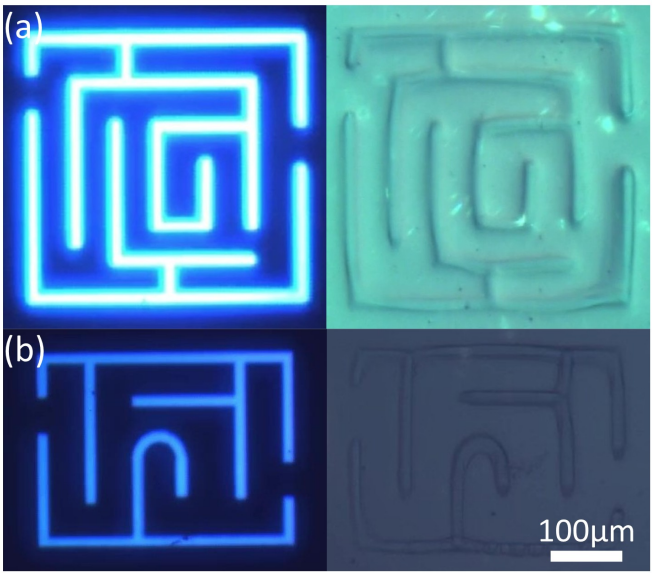

Fig. 7. Customized hydrogel maze microstructures generated via OET: (a) square maze, (b) rectangular maze.

- **Square maze**: 400 μm $\times$ 400 μm, containing multiple nested spiral channels (Fig. 7a). By projecting blue light patterns precisely matching the maze contours via the DMD, hydrogel solidification was completed within 6 minutes. The channels exhibited uniform widths (approximately 15 μm), and the geometric deviations between nested layers were less than 10%.
- **Rectangular maze**: 250 μm $\times$ 400 μm, with channels including curved turns and other complex structures (Fig. 7b). Using the programmable light patterns of OET, solidification was achieved within 6 minutes, with smooth transitions in curved channels and deviations from the design contour below 10 μm.

These experiments demonstrate that OET not only enables precise single-region microstructure fabrication but also supports large-area batch production and customizable construction of complex topologies. This provides a stable and predictable physical environment for hydrogel-based dynamic microparticle manipulation. Moreover, by circumventing the reliance on conventional photolithography templates, the method establishes an integrated experimental strategy of "high-precision static structure generation–dynamic microparticle control," laying a technical foundation for large-scale and personalized hydrogel microstructures in biomedical applications.

D. Microsphere Navigation in Hydrogel Maze Structures

Following the fabrication of static and customized hydrogel microstructures, we further evaluated the capability of OET to precisely manipulate single and multiple microspheres within hydrogel carriers. The rectangular maze (250 μm $\times$ 400 μm) served as the physical substrate. PS microspheres (15 μm) were dispersed in GelMA–LAP precursor solution (conductivity 28.4 μS/cm), and light patterns with wavelengths $\geq$580 nm were projected to generate dielectrophoretic forces for particle motion control without inducing additional hydrogel crosslinking. The applied AC voltage was 15 Vpp at 1 MHz for all experiments.

1) Single-Particle Maze Navigation: Single-particle manipulation focused on verifying path accuracy. A solid square light pattern (80 μm side length) was projected via DMD as the DEP-inducing source. The non-uniform electric field within the illuminated region captured the PS microsphere and guided it along the hydrogel maze channel from the right starting point to the left endpoint (Fig. 8a).

The integrated trajectory map clearly shows the complete path: start point localization, mid-path turns and obstacle avoidance, and arrival at the endpoint. The velocity-time profile (Fig. 9d) indicates dynamic velocity adjustments under DEP forces, with an average speed of 10.887 μm/s. The particle traversed the approximately 950 μm maze path within 89 s, maintaining path deviations below 15 μm. This demonstrates that OET enables low-disturbance, high-precision single-particle control within a hydrogel environment. The solidified hydrogel channels provide physical constraints that reduce Brownian motion-induced deviations, significantly enhancing manipulation stability.

2) Dual-Particle Coordinated Maze Navigation: Dual-particle manipulation emphasized synchronization. A single solid circular light pattern (diameter 60 μm) first captured the leading particle via DEP. The secondary particle was subsequently guided through inter-particle DEP interactions, enabling synchronous movement. Trajectories (Fig. 9b) showed high overlap along the maze path. Velocity profiles (Fig. 9e) indicated average speeds of 10.692 μm/s and 9.352 μm/s for the leading and following particles, respectively (87.5% of the leader), confirming synchronized motion.

Real-time CCD tracking allowed dynamic adjustment of

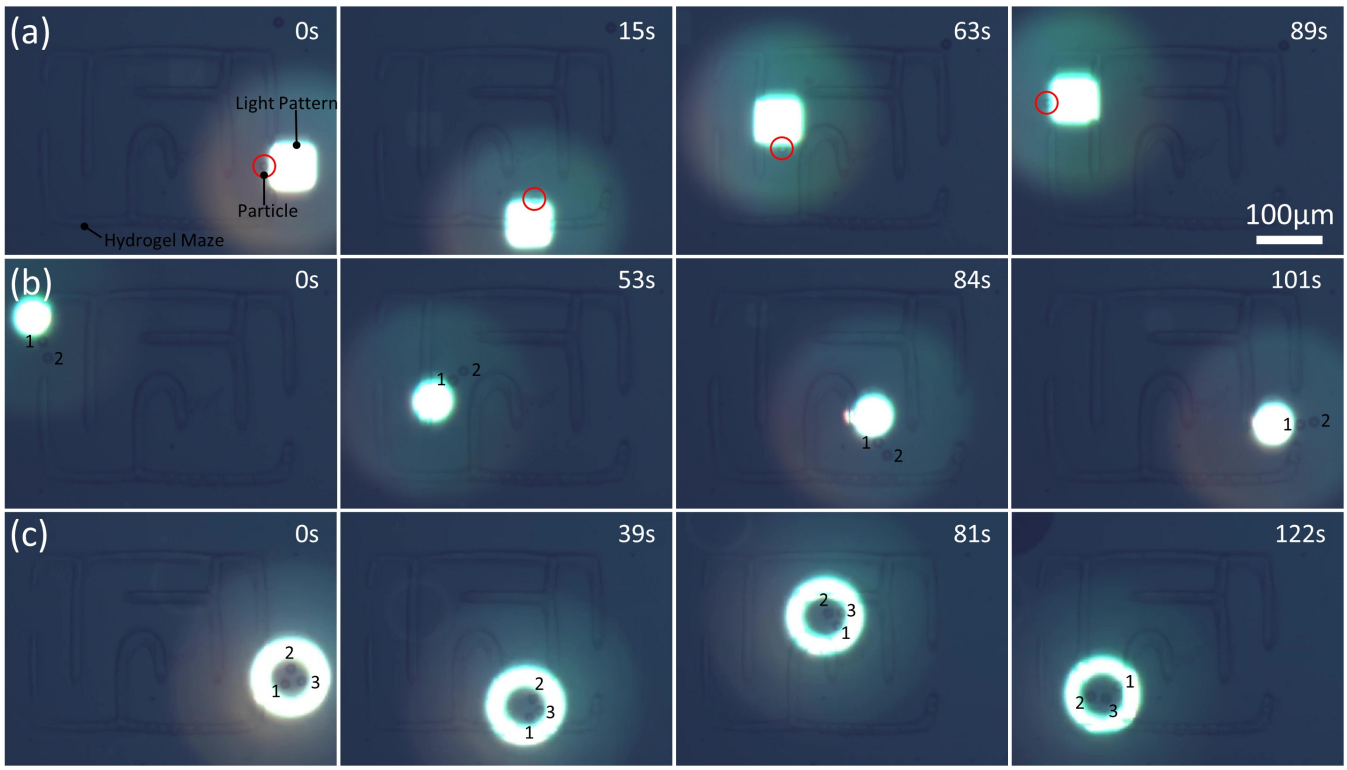

Fig. 8. Trajectories of PS microspheres navigating within hydrogel maze structures: (a) single-particle navigation, (b) dual-particle coordinated navigation, (c) triple-particle synchronized navigation.

the light pattern to maintain inter-particle distances below 15 μm, with fluctuations within 5 μm. The dual particles completed the approximately 950 μm path within 101 s. These results demonstrate that OET can precisely regulate inter-particle interactions, enabling coordinated multi-particle navigation in hydrogel mazes, which is relevant for tasks such as cooperative biomolecule transport.

3) Triple-Particle Coordinated Maze Navigation: Triple-particle manipulation validated higher-order coordination using a hollow circular light field (inner diameter 60 μm, outer diameter 100 μm). The hollow light pattern created uniform DEP capture forces for all three microspheres while minimizing interference in relative positions. Trajectories (Fig. 9c) show that the three particles maintained a triangular formation while moving along the maze centerline. Velocity profiles (Fig. 9f) indicate average speeds of 6.454 μm/s, 6.740 μm/s, and 7.309 μm/s, with differences below 0.9 μm/s, demonstrating synchronized motion.

Real-time adjustments of the hollow light field ensured the triangular formation was maintained throughout the narrow channels. The triple particles traversed approximately 800 μm within 122 s without leaving the manipulation region.

Overall, these experiments demonstrate that hydrogel-patterned structures provide physical constraints and movement channels, and combined with programmable OET light patterns, enable full control from single-particle path accuracy to multi-particle coordination. This integrated "static structure–dynamic control" strategy overcomes the tradi-

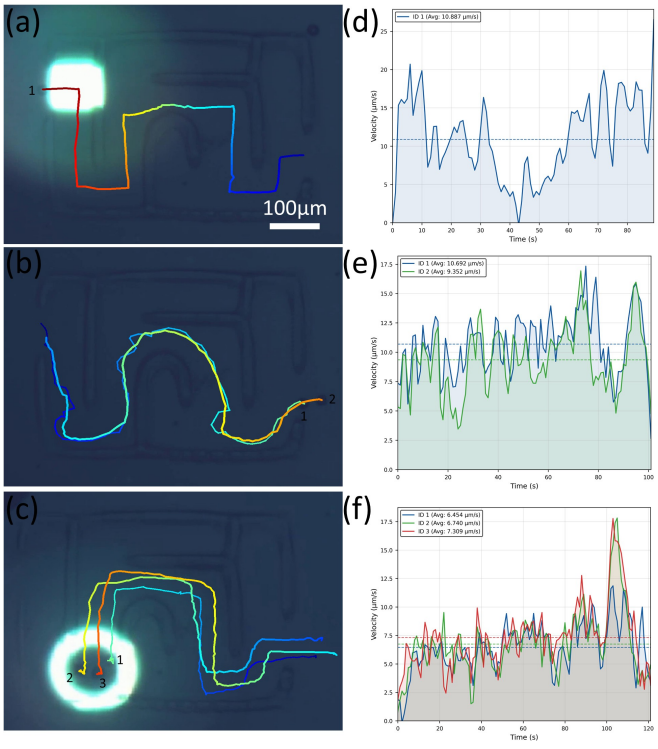

Fig. 9. PS microsphere navigation within hydrogel maze structures: (a) single-particle trajectory, (b) dual-particle trajectory, (c) triple-particle trajectory; (d) single-particle velocity profile, (e) dual-particle velocity profile, (f) triple-particle velocity profile.

tional separation of microchannel fabrication and particle manipulation in hydrogel microenvironments, providing a reproducible platform for tissue engineering and targeted particle transport applications.

IV. CONCLUSIONS

In this study, we addressed the environmental limitations and workflow fragmentation associated with OET in microscale particle manipulation by developing an integrated platform employing a dual-wavelength optical strategy. This approach enabled high-precision control of microspheres in both aqueous and hydrogel environments.

In the aqueous phase, 15 μm PS microspheres were pre-aggregated to form well-defined patterns with edge roughness below 20 μm, demonstrating the high-fidelity patterning capability of OET. For hydrogel static fabrication, biocompatible GelMA–LAP was used as the precursor, and 365–405 nm light induced polymerization to generate single-region, batch, and complex-topology microstructures. The hexagram pattern exhibited 100% contour fidelity, with a maximum deviation of only 10.458 μm, confirming that OET can construct precise biocompatible microstructures.

For dynamic manipulation within hydrogels, light with wavelengths $\geq$580 nm drove dielectrophoretic motion to achieve maze navigation of single, dual, and triple microspheres. Single-particle paths maintained deviations below 15 μm, dual particles maintained inter-particle distance fluctuations below 5 μm, and triple particles exhibited velocity differences under 0.9 μm/s, validating the stability and precision of coordinated multi-particle control.

Overall, this study presents a maskless, integrated micromanipulation strategy that combines biocompatibility with programmability. It provides a reproducible and operable experimental platform for tissue engineering microenvironments, targeted particle delivery, and multi-particle cooperative tasks, thereby expanding the application scope of OET in biomedical research.

ACKNOWLEDGMENT

Thanks to the Center for Micro-Nano Innovation at Beihang University (Beihang Nano) for help with device fabrication.

REFERENCES

[1] S. Zhang, B. Xu, M. Elsayed, F. Nan, W. Liang, J. K. Valley, L. Liu, Q. Huang, M. C. Wu, and A. R. Wheeler, "Optoelectronic tweezers: a versatile toolbox for nano-/micro-manipulation," *Chemical Society Reviews*, vol. 51, no. 22, pp. 9203–9242, 2022.

[2] Y. Huang, Z. Liang, M. Alsoraya, J. Guo, and D. Fan, "Light-gated manipulation of micro/nanoparticles in electric fields," *Advanced Intelligent Systems*, vol. 2, no. 7, p. 1900127, 2020.

[3] H. Xie and X. Ding, "The intriguing landscape of single-cell protein analysis," *Advanced Science*, vol. 9, no. 12, p. 2105932, 2022.

[4] P. Y. Chiou, A. T. Ohta, and M. C. Wu, "Massively parallel manipulation of single cells and microparticles using optical images," *Nature*, vol. 436, no. 7049, pp. 370–372, 2005.

[5] B. Xu, Y. Zhao, X. Chen, R. Fu, H. Li, S. Xie, H. Liu, Y. Li, S. Zhang, and B. Li, "Power micromachines with light," *Laser & Photonics Reviews*, vol. 19, no. 4, p. 2400791, 2025.

[6] A. Wang, S. Liang, C. Ni, Y. Jia, K. Wu, W. Niu, S. Huang, K. Peng, C. Wang, Y. Guo *et al.*, "Particle-assisted optoelectronic tweezers for manipulating single cells and microparticles," *Advanced Science*, p. 2501032, 2025.

[7] S. Huang, J. Zhao, C. Gan, Z. Zeng, H. Xiong, J. Ye, W. Niu, A. Wang, C. Li, H. Sun *et al.*, "High-precision parallel manipulation of multi-particle system using optoelectronic tweezers," in *2025 IEEE/RSJ International Conference on Intelligent Robots and Systems (IROS)*. IEEE, 2025, pp. 11 484–11 489.

[8] S. Liang, J. Sun, C. Zhang, Z. Zhu, Y. Dai, C. Gan, J. Cai, H. Chen, and L. Feng, "Parallel manipulation and flexible assembly of micro-spiral via optoelectronic tweezers," *Frontiers in bioengineering and biotechnology*, vol. 10, p. 868821, 2022.

[9] S. Huang, J. Zhao, C. Gan, Z. Zeng, H. Xiong, J. Ye, H. Sun, W. Niu, A. Wang, C. Li *et al.*, "Optoelectronic tweezers platform for label-free and automated multidimensional sperm manipulation," *Advanced Materials Technologies*, p. e01167, 2025.

[10] S. Liang, C. Gan, Y. Dai, C. Zhang, X. Bai, S. Zhang, A. R. Wheeler, H. Chen, and L. Feng, "Interaction between positive and negative dielectric microparticles/microorganism in optoelectronic tweezers," *Lab on a Chip*, vol. 21, no. 22, pp. 4379–4389, 2021.

[11] G. Li, B. Xu, X. Wang, J. Yu, Y. Zhang, R. Fu, F. Yang, H. Gu, Y. Huang, Y. Chen *et al.*, "Crossing the dimensional divide with optoelectronic tweezers: Multicomponent light-driven micromachines with motion transfer in three dimensions," *Advanced Materials*, vol. 37, no. 17, p. 2417742, 2025.

[12] J. Zhao, B. Chen, C. Gan, S. Huang, H. Xiong, J. Ye, P. Zhang, and L. Feng, "Study of particle equilibrium based on the combination of light-actuated ac electroosmosis and light-actuated dielectrophoresis," *Optics Express*, vol. 32, no. 14, pp. 24 563–24 572, 2024.

[13] L. Zheng, G. Li, H. Du, Z. Li, B. Xu, F. Yang, Y. Mao, J. Wei, H. Xie, W. Xie *et al.*, "Automated and collision-free navigation of multiple micro-objects in obstacle-dense microenvironments using optoelectronic tweezers," *Microsystems & Nanoengineering*, vol. 11, no. 1, p. 49, 2025.

[14] S. Zhang, M. Elsayed, R. Peng, Y. Chen, Y. Zhang, J. Peng, W. Li, M. D. Chamberlain, A. Nikitina, S. Yu *et al.*, "Reconfigurable multi-component micromachines driven by optoelectronic tweezers," *Nature communications*, vol. 12, no. 1, p. 5349, 2021.

[15] J. Zhao, C. Gan, J. Zhang, S. Liang, J. Yang, and L. Feng, "Deep learning assisted automated separation platform of single cells and microparticles using optoelectronic tweezers," in *2022 WRC Symposium on Advanced Robotics and Automation (WRC SARA)*. IEEE, 2022, pp. 275–279.

[16] Y. Zhao, K. Lin, H. Yang, X. Dong, T. Sun, Q. Shi, Q. Huang, and H. Wang, "Deep learning-guided single-cell encapsulation through photo-crosslinking for advanced 3d culture," in *2024 IEEE International Conference on Mechatronics and Automation (ICMA)*. IEEE, 2024, pp. 1831–1836.

[17] S. Wang, W. Liang, Z. Dong, V. G. Lee, and W. J. Li, "Fabrication of micrometer-and nanometer-scale polymer structures by visible light induced dielectrophoresis (dep) force," *Micromachines*, vol. 2, no. 4, pp. 431–442, 2011.

[18] W. Wang, Z. Gao, X. Feng, X. Teng, Z. Qiao, Z. Ge, Q. Fan, and W. Yang, "The customized design and fabrication of microchannels via optically induced dielectrophoresis for particle manipulation," *Nanotechnology and Precision Engineering*, vol. 8, no. 3, 2025.

[19] S. Xiao, T. Zhao, J. Wang, C. Wang, J. Du, L. Ying, J. Lin, C. Zhang, W. Hu, L. Wang *et al.*, "Gelatin methacrylate (gelma)-based hydrogels for cell transplantation: an effective strategy for tissue engineering," *Stem cell reviews and reports*, vol. 15, no. 5, pp. 664–679, 2019.

[20] G. Ying, N. Jiang, C. Yu, and Y. S. Zhang, "Three-dimensional bioprinting of gelatin methacryloyl (gelma)," *Bio-Design and Manufacturing*, vol. 1, no. 4, pp. 215–224, 2018.

[21] S. Neale, M. Mazilu, J. Wilson, K. Dholakia, and T. Krauss, "The resolution of optical traps created by light induced dielectrophoresis (lidep)," *Optics express*, vol. 15, no. 20, pp. 12 619–12 626, 2007.

[22] P. R. Gascoyne and J. Vykoukal, "Particle separation by dielectrophoresis," *Electrophoresis*, vol. 23, no. 13, p. 1973, 2002.